0888-8809/08/$15.00/0
Printed in U.S.A.

Molecular Endocrinology 22(7):1565–1578

doi: 10.1210/me.2007-0501

Ligand Dissociation from Estrogen Receptor Is Mediated by Receptor Dimerization: Evidence from Molecular Dynamics Simulations

Milton T. Sonoda, Leandro Martínez, Paul Webb, Munir S. Skaf, and Igor Polikarpov

Instituto de Física de São Carlos (M.T.S., I.P), Universidade de São Paulo, São Carlos SP 13560-970, Brazil; Instituto de Química (L.M., M.S.S), Universidade Estadual de Campinas-UNICAMP, Campinas SP 13084-862, Brazil; and Methodist Hospital Research Institute (P.W.), Houston, Texas 77030

Estrogen Receptor (ER) is an important target for pharmaceutical design. Like other ligand-dependent transcription factors, hormone binding regulates ER transcriptional activity. Nevertheless, the mechanisms by which ligands enter and leave ERs and other nuclear receptors remain poorly understood. Here, we report results of locally enhanced sampling molecular dynamics simulations to identify dissociation pathways of two ER ligands [the natural hormone 17β-estradiol (E_2) and the selective ER modulator raloxifene (RAL)] from the human ERα ligand-binding domain in monomeric and dimeric forms. E_2 dissociation occurs via three different pathways in ER monomers. One resembles the mousetrap mechanism (Path I), involving repositioning of helix 12 (H12), others involve the separation of H8 and H11 (Path II), and a variant of this pathway at the bottom of the ligand-binding domain (Path II′). RAL leaves the receptor through Path I and a Path I variant in which the ligand leaves the receptor through the loop region between H11 and H12 (Path I′). Remarkably, ER dimerization strongly suppresses Paths II and II′ for E_2 dissociation and modifies RAL escape routes. We propose that differences in ligand release pathways detected in the simulations for ER monomers and dimers provide an explanation for previously observed effects of ER quaternary state on ligand dissociation rates and suggest that dimerization may play an important, and hitherto unexpected, role in regulation of ligand dissociation rates throughout the nuclear receptor family. (*Molecular Endocrinology* 22: 1565–1578, 2008)

THE NUCLEAR RECEPTOR (NR) superfamily comprises transcription factors that are mostly activated by small hydrophobic molecules, including endocrine hormones, vitamins, and secondary metabolites, and play important roles in major physiological processes such as development, metabolism, and homeostasis (1).

The estrogen receptor (ER) and its cognate hormone 17β-estradiol (E_2, Fig. 1) are important for female health and well-being (2–4). Abnormal ER activity is associated with breast cancer, which is often treated with synthetic competitive inhibitors of E_2 binding, such as faslodex, tamoxifen, and raloxifene (RAL, Fig. 1). RAL is a selective ER modulator (SERM), which functions as an antagonist in breast and an agonist in other tissues, including bone, and has important potential applications in breast cancer and osteoporosis therapy (3, 5).

NRs have modular structures with an N-terminal domain, the DNA-binding domain, and the C-terminal ligand-binding domain (LBD) (6). The LBD also harbors cofactor binding sites, including a hormone-dependent activation function-2 and surfaces that mediate dimerization, which, for ER, is needed for optimal transcriptional activation.

Hormone binding activates ER by altering LBD conformation. Unliganded (apo) NRs adopt mobile and partially disordered globular states that rearrange in response to ligand (7, 8). Agonists trigger multiple conformational changes required for dimerization, nuclear translocation, DNA binding, and recruitment of the cellular transcription machinery. Of these events, the best characterized is enhanced packing of LBD C-terminal helix 12 (H12) against H3 and H5 to form activation function-2, which comprises a hydrophobic cleft that interacts with NR coactivators (9). Antagonists or SERMs such as RAL contain a large molecular extension that prevents docking of H12 into the active conformation, inhibiting coactivator binding, and sometimes promoting recruitment of corepressors (10). Thus, ligand determines H12 conformation, and this event functions as a molecular switch of NR activity.

First Published Online April 10, 2008

Abbreviations: E_2, 17β-Estradiol; ER, estrogen receptor; H12, helix 12; LBD, ligand-binding domain; LES, locally enhanced sampling; MD, molecular dynamics; NR, nuclear receptor; RAL, raloxifen; RAR, retinoic acid receptor; SERM, selective ER modulator; TR, thyroid hormone receptor.

***Molecular Endocrinology* is published monthly by The Endocrine Society (http://www.endo-society.org), the foremost professional society serving the endocrine community.**

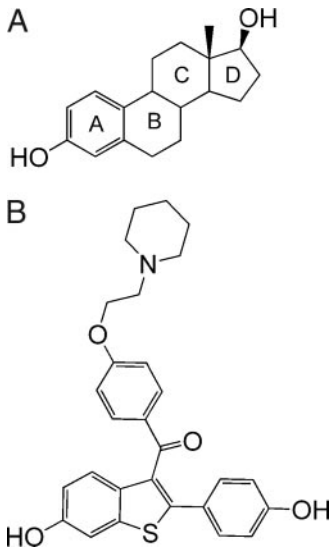

Fig. 1. Structures of ER Ligands
E_2 (panel A) and RAL (panel B).

X-ray structures of holo-NR-LBDs show that ligands are buried in the hydrophobic core of the protein, with no obvious entry or exit routes. Hence, significant LBD conformational rearrangements must accompany ligand entry into and escape from its binding site. Knowledge of these rearrangements may open new perspectives for pharmacological drug design.

Analysis of an unliganded NR-LBD structure, retinoic X receptor-α (Protein Data Bank identification: 1LBD) revealed that H12 adopts an open conformation away from the body of the receptor. This led to the suggestion, termed the "mousetrap" mechanism, that repositioning of H12 opens the entry and exit route for the buried pocket (11). In accordance with this model, ligand affinity increases in the presence of coactivators, which lock H12 in the active position. The mousetrap model nevertheless remains controversial. H12 adopts the closed active conformation in other apo-NR-LBD structures, including peroxisomal proliferator-activated receptor (12) and estrogen-related receptor 2 with and without (13) coactivator peptides (14) and the orphan receptors Nurr77 (15) and DHR38 (16).

We and others suggested that NR-LBDs may harbor alternate ligand escape routes. Analysis of temperature factors (B factors) of NR-LBD x-ray structures, which provide an indirect index of mobility, reveals that the H1–H3 loop regions and associated β-sheets are highly flexible and may constitute an alternative ligand entry/exit route (17). In addition, molecular dynamics (MD) computer simulations revealed multiple pathways for ligand binding and release. Several groups analyzed retinoid release from retinoic acid receptors (RARs); one study observed ligand can escape under H12, similar to the mousetrap mechanism (18) whereas others observed ligand escape through expansion of the H1–H3 loop and associated β-hairpin (19, 20). We detected three possible ligand escape paths from thyroid hormone receptor (TR) LBDs (21, 22): Path I involves dislocation of H12 from H3 and H11 (see Fig. 2 and also Fig. 3 of Ref. 21), Path II is formed by the joint displacement of H8, H11, and the associated β-loop, and Path III involves a hydrophilic cavity formed by the rearrangements in the H1–H3 loop and the β-sheet (21). We proposed that the latter is most favorable, *i.e*. it involves rearrangements that result in interaction of the hydrophilic polar end of ligands with external water molecules, and this occurs at little energetic cost (22).

The notion that NR-LBDs harbor multiple ligand escape routes raises the possibility that many factors could regulate ligand dissociation rates with concomitant effects on ligand affinity and/or kinetic stability of the complex. Hormone binding is stabilized by association with coactivator, and *vice versa*, with stabilization of the receptor-ligand-coactivator complex (23). Influences of dimer formation, which involves a large interface that overlaps H8, H9, H10, and H11 (24), are less clear. Here, we report results of locally enhanced sampling (LES) MD simulations to assess likely pathways of E_2 and RAL (Fig. 1) dissociation from the ERα-LBD in monomeric and dimeric form. We observe pathways that resemble Path I and Path II, described above and schematically depicted in Fig. 2. We also find that dissociation pathways depend on both the

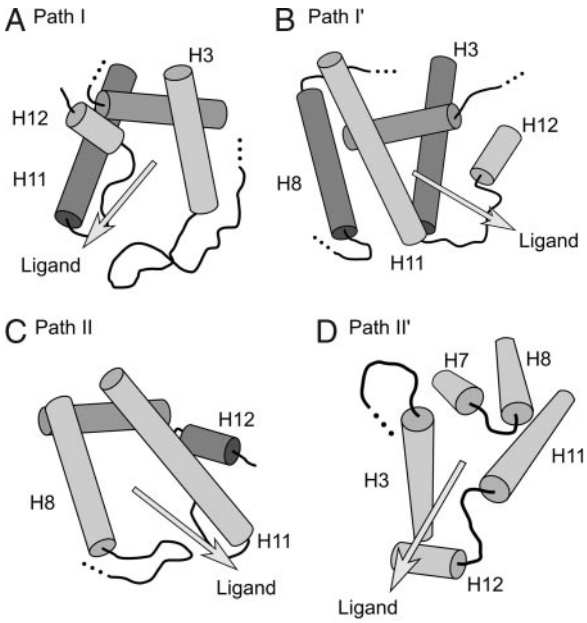

Fig. 2. Schematic Representation of the Four Paths Found
A, Path I is the classical mousetrap mechanism, in which the ligand dissociates within H3 and H12. B, In Path I′ the displacement of H12 occurs above H3, and the ligands dissociate between H12 and H11. C, In Path II an aperture between H8 and H11 opens the binding pocket leading to ligand dissociation. D, In Path II′, ligand dissociates through the bottom of the LBD, which can be viewed as an extrapolation of Path II (or Path I) over the *lower part* of the LBD.

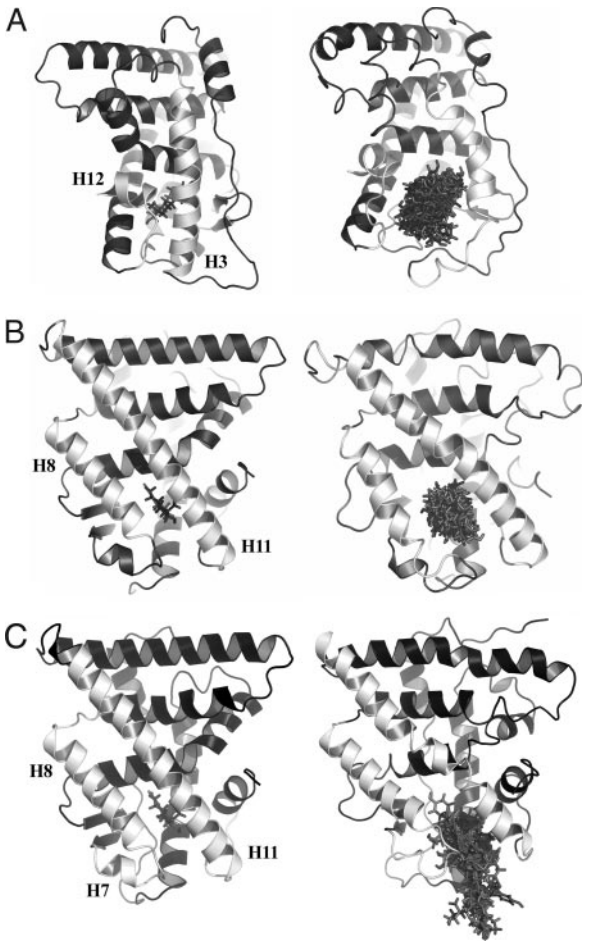

Fig. 3. Main Structural Rearrangements of ER-LBD/E_2 in Monomeric State that Accompany E_2 Escape

In *light gray* are the helices involved in the cavity formation. The *figures on the left* show views of the crystallographic structure with these helices in first plane. *On the right* are snapshots of the simulations showing the arrangements on these helices responsible for escape cavity formation. A, Escape cavity formation through path I between H3, H12, and H11–H12 loop. B, Escape cavity formation through path II between N terminus of H8 and C terminus of H11. C, Escape cavity formation through path II′, at the *bottom* of the LBD.

ligand and ER quaternary state. Our results may explain previously published experimental data, which show that ER dimer formation regulates ligand binding and dissociation rates, and we discuss our findings in terms of synthetic ligand design for ERs and other NRs.

RESULTS

Three Pathways for E_2 Dissociation from ER-LBD Monomers

We performed three sets of LES simulations for ERα-LBD monomers in vacuum with 50, 40, and 30 copies of E_2. In LES simulations, interactions of multiple copies of the same ligand with the receptor are computed simultaneously to enhance the likelihood of dissociation events during the short time frame of the simulation. Two different escape routes were observed: Paths I and II, schematically represented in Fig. 2, A and C. In Path I, the ligands dissociate from ER-LBD through a space opened between H12 and H3, with corresponding secondary structures of both helices largely preserved. In Path II, the separation of H8 and H11 at the lower part of ER-LBD (near the H11 C terminus) allows for ligand dissociation. Similar paths were previously detected in our studies of ligand dissociation from TR-LBDs (21). Path I was also encountered in the earlier LES study of retinoic acid-RAR dissociation (18). The third, and most favorable, ligand escape route found in our simulations of TR-LBDs (Path III, an aperture between H3, H1–H2 loop, and the β-sheets, as shown in Fig. 3 of Ref. 21), was not observed.

Path II was observed most frequently with ER-E_2 monomers (Table 1). This was the only escape route observed with 50 copies and predominated in simulations with 30 and 40 copies. Path I was observed only twice, once with 40 copies and again with 30 copies. Several simulations performed with 30 copies failed to yield ligand release within the simulated time window.

To assess possible effects of solvent on the dissociation pathways, we performed additional LES simulations with structures that include crystallographic waters. Here, a third escape route closely related to Path II was observed. This route (Path II′) has never been observed in other MD investigations of ligand dissociation from NR-LBDs and is schematically depicted in Fig. 2D. It involves near complete unfolding of the short H7 and loss of contact with N terminus of H11, opening the binding pocket and allowing the escape of ligand copies. Further assessment of solvent effects was obtained from simulations with a full hydration shell and is discussed separately (see Fig. 9).

E_2 Escape Cavities in ER-LBD Models

In this section we describe early events of ER-LBD dynamics responsible for E_2 dissociation. We focus on the global ER-LBD structural fluctuations and disruption of specific residue contacts that form the escape cavity. For clarity, we compare native structural features of specific LBD regions with their counterparts at the early stages of the LES simulations, *i.e*. before trajectories of multiple ligands used in the simulation start diverging, to identify key protein-protein noncovalent contacts that are ruptured to form the initial surface aperture that allows for ligand escape.

Table 1. Number of Observed Dissociation Events through Each Path for the E_2 and RAL Ligands from ER-LBD in Monomeric and Dimeric States with Varying Number of Ligand Copies in LES Simulations

No. of Copies	ER Monomer/E_2				ER Monomer/RAL		
	Path I	Path II	Path II′	No Dissociation	Path I/I′	Path II′	No Dissociation
50	0	7	0	0	4[b]/1[c]	0	0
40	1	7	0	0	4/1	0	0
30	1	4	0	4	5/0	0	0
50[a]	0	0	2	2	4/0	0	0
			ER dimer/E_2			ER dimer/RAL	
50	7	0	0	5	7[d]/6[d,e]	2	0
30	7	0	0	7	2/5	4	0
20	2	0	0	7	1/4[f]	1	1
50[a]	2	0	0	2	0/4	0	0

The sum of dissociation and no-dissociation events equals the number of simulations performed in each case.
[a] Simulations in the presence of crystallographic waters.
[b] In one simulation most of the copies escaped through Path I, whereas a few copies escaped through Path I′.
[c] In one simulation most of the copies escaped through Path I′, whereas a few ligand copies escaped through Path I.
[d] In two simulations nearly the same amount of ligand copies escaped through Paths I and I′.
[e] In one simulation most of the copies escaped through Path I′, whereas a few ligand copies escaped through Path II′.
[f] In one simulation nearly the same amount of copies escaped through Paths I′ and II′.

Dissociation along Path I

Initially, the H11–H12 loop lies nearly parallel to H3, and there are several contacts between this region and H12 with H3 and H5 closing the pocket (Fig. 3A and 4A, *left*). First, there is partial unfolding of the N-terminal region of H3 between amino acids M342 and L346. This region of H3 forms part of the hydrophobic cleft where H12 docks in its agonist conformation and the L346 side chain makes hydrophobic contacts with E_2. The next step is the breakage of hydrophobic contacts between residues in H3 and the H11–H12 loop. After loss of these contacts, the H11–H12 loop and the N-terminal part of H12 move outward, forming a cavity between the H11–H12 loop and the N-terminal part of H3, allowing the ligand to escape. A very similar event of H3 partial unfolding has been observed in LES simulations of ligand dissociation from TR-LBD (21).

The details of Path I escape cavity and important residues involved are shown in Fig. 4A. The cavity is formed by disruption of hydrogen bonding between N348 in H3 and Y537 in the H11–H12 loop; D351 in H3 and the L540 backbone amide hydrogen in H12; and several hydrophobic interactions [V355 and L354 (H3) with L539 (H12) and T347 (H3) with L540 and P535 (H12)].

Dissociation along Path II

The main feature of ligand (E_2) dissociation along Path II is detachment of H8 and H11 after partial unwinding of the N-terminal region of H8 and/or C-terminal region of H11 (Figs. 3B and 4B). There are several side chain interactions that maintain the close proximity and antiparallel orientation of H8 and H11. The formation of the escape cavity starts with disruption of the contacts between residues lying on the C terminus of H11 and the N terminus of H8, and concomitant unwinding of H8 and/or H11. Some residues of this region of H8 and H11 make direct contacts with the ligand and H12, *e.g*. H524, which hydrogen bonds with the D-ring hydroxyl of E_2 (Fig. 1A). The final step is the separation of the unwound part of H8 from H11 at the lower part of ER-LBD, opening the cavity for ligand dissociation (Fig. 3B).

The details of Path II escape cavity and important residues involved are depicted in Fig. 4B. The cavity is formed by disruption of a salt bridge between E419 in H8 and K531 in H11, disruption of a hydrogen bond between E419 backbone carbonyl and H524, and breakage of some hydrophobic contacts, namely M427 (H8) and M517 (H11), and I424 and M427 (H8) with the hydrophobic part of the K520 side chain (H11).

Dissociation along Path II′

The main feature of this escape pathway is unfolding of the short helix, H7, at the bottom of the LBD. H7 is folded and the H7–H8 loop and C terminus of the H2–H3 loop are held together through a hydrogen bond between the backbone nitrogen of E419 and E339 side chain. In addition, a salt bridge between E419 and K531 maintain close contact between the H7–H8 loop and the C terminus of H11. These interactions maintain closed the Path II′ escape route.

The molecular events related to Path II′ escape cavity formation are shown in Fig. 3C. The binding pocket exposure involves almost complete unfolding of H7 and the concomitant loss of interaction between the H7–H8 loop and the C terminus of the H2–H3 loop. The latter event allows for the N terminus of H3 to detach from H8 and H11, opening the escape cavity. This escape route is also observed in simulations with RAL, with similar molecular details of cavity formation, as discussed below.

E_2 Dissociation from ER-LBD through Paths II and II′ Are Suppressed in Homodimers

Because the ER dimerization surface is comprised of residues on the surface of H8 and H11, the fact that ligand release occurs through Path II in ER monomers is highly suggestive of a relationship between LBD dimerization and ligand release. We performed several simulations of E_2 dissociation from structural models of an ER-LBD dimer with varying number of ligand copies in the presence and absence of crystallographic waters. Unlike results with ER-LBD monomers, Path I was the only route for E_2 dissociation in these simulations (Table 1). The structural rearrangements that culminate in escape cavity formation are similar to those found in the ER-LBD monomer (Fig. 5). Equally interesting is the fact that E_2 failed to dissociate at all in nearly 50% of the ER dimer simulations, as opposed to the monomers in which dissociation events were more common.

RAL Dissociation from ER Monomer Occurs through Escape Routes Involving H12

MD simulations with models of the ER-RAL monomer complex revealed differences from ligand escape paths obtained with E_2. We performed three sets of five independent LES simulations in vacuum with 50, 40, and 30 ligand copies each, and an additional set with 50 copies and crystallographic waters. In most simulations, we observed ligand dissociation through a pathway similar to Path I. Less frequently, we also observed RAL release through a related route (Path I′) in which the ligand passes above the H11–H12 loop (Fig. 2). The main event that accompanies RAL dissociation through both paths is near complete unfolding of H12, shown in Fig. 6, A (Path I) and B (Path I′).

Details of the cavity formation and specific residues are presented in Fig. 7, A and B. In the beginning of the simulation, H12 adopts the antagonist position and participates in hydrophobic interactions with H3 and H5, whereas the RAL molecular extension protrudes over H12 interacting with D531 at H3 (*left panels* of Figs. 6A and 7A). In Path I, the escape cavity is associated with H12 unfolding and disruptions of these interactions, leading to ligand dissociation. For Path I′, in addition to H12 unfolding, RAL dissociation is characterized by partial unfolding of the H11 C-terminal part of H11 and concomitant reorientation of the ligand molecular extension over the H11–H12 loop (Fig. 6B). During cavity formation, there are disruptions of interactions between L354 in H3 with L536, L539 and M543 in H12, I358 (H3) with M543 and L544 (H12), L541 and L544 (H12) with L372, and V376 and L379 (H5) (Fig. 7B).

Multiple Pathways Are Involved in RAL Dissociation from ER Dimers

Paths I and I′ of RAL unbinding from ER-LBD monomers were also observed in dimers (Fig. 8, A and B) and involved very similar events. However, a third dissociation path (Path II′) for RAL, similar to that found for E_2 in ER monomer, was observed relatively frequently for the ER dimer. This pathway involves unfolding of H7 and partial unfolding of part of the H11 C terminus (Fig. 8C) with details of the initial aperture on the protein surface associated with this unbinding pathway shown in Fig. 7C. Different from the ligand unbinding events discussed so far, the simulations reveal no clear prevalence of a single dissociation path for RAL in ER-LBD dimers, with all pathways frequently detected (Table 1). Inspection of crystallographic structures and the simulation trajectories reveals differences in organization of E_2 and RAL dissociation routes from ER monomers and dimers. For E_2, the secondary structure elements that surround the Path II′ cavity are the C terminus of the H2–H3 loop, the N terminus of H3, H7, H7–H8 loop, the C terminus of H11, and the H11–H12 loop, which also participates in Path I. These structures are also involved in Path II′ for RAL, with the sole exception of the H11–H12 loop, which adopts an alternative conformation in ER+RAL complex as a result of the H12 antagonist conformation. We propose this variation may account for some differences in ligand release pathways observed with E_2 and RAL (see *Discussion*).

Fully Solvated Systems

To examine effects of solvent on dissociation pathways, we performed longer (3–5 nsec) LES simulations of E_2 and RAL complexed to ER in monomeric and dimeric states in the presence of a thick (15Å) solvation layer containing several thousand water molecules (see *Materials and Methods*). Under full solvation conditions no ligand dissociation events were observed during the simulation time for all systems and, not surprisingly, the protein structures remained largely preserved. However, these simulations reveal early molecular events associated with transient formation of cavities on the surface of the protein connecting the ligand binding pocket to the bulk solvent (Fig. 9). Strikingly, these cavities appear at the same regions of the escape routes discussed above, and nowhere else on the protein surface. Specifically, a cavity is observed in the Path II and II′ region for the monomeric E_2/ER (Fig. 9A). For the monomeric RAL/ER complex a cavity is observed in the region of Path I (Fig. 9B), whereas in dimeric RAL/ER complex, a large cavity is formed in the region of Path II′ (Fig. 9C). Hence, LES simulations employing full solvation provide important support for results obtained with simulations performed *in vacuo* or with crystallographic waters: every cavity observed in simulations in the presence of solvent has a dissociation counterpart in simulations performed in vacuum or with structural waters.

DISCUSSION

In this work, we applied LES simulations to investigate pathways of E_2 and RAL dissociation from structural

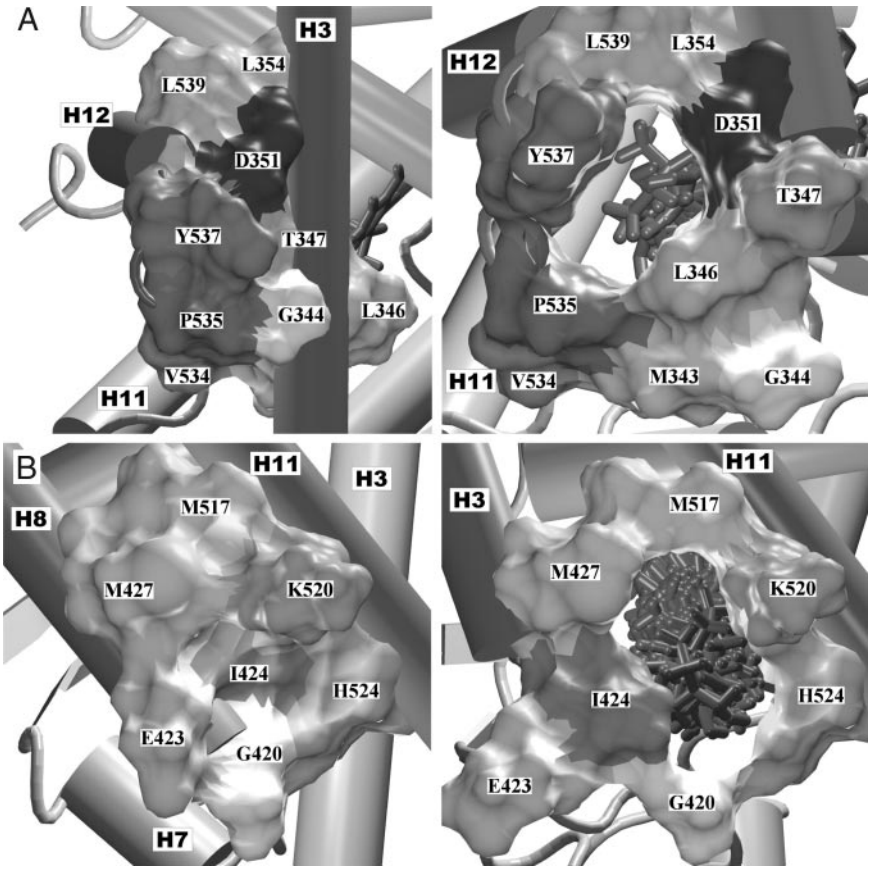

Fig. 4. Details of the E_2 Escape Cavity Formation from ER-LBD

The main structure of the protein is shown in *cartoon* representation and the residues involved in cavity formation are labeled and shown as surfaces. On the *left* are crystallographic views of the structure, and on the *right* are snapshots of the initial stages of the cavity formation. A, Cavity for escape through path I. For the sake of clarity V355, which lies in front of L354, is not shown. The L540 mentioned in the text is *above* D351 and Y537. B, Cavity for escape through path II.

models of ER-LBD in monomeric and dimeric states. In agreement with previous studies of TRs, we observe multiple ligand escape paths. The route varies according to the quaternary state of the receptor and ligand. In ER monomer simulations with E_2, three dissociation pathways were identified. The most frequent involves an aperture between H8 and H11 (Path II), as previously seen with the TR-LBD (21). Less frequently, E_2 dissociates through displacement of H12 (Path I), similar to the mousetrap model observed in simulations of RAR (18–20) and TR-LBDs (21, 22). Simulations with structural waters reveal a novel escape route: through the bottom of the LBD after H7 unfolding (Path II′). Paths II and II′ were suppressed in ER dimers and, in general, ligand escape was observed less frequently in dimers. By contrast, simulations with RAL-ER monomers only detected both variants of the mousetrap model (Paths I and I′). These paths also predominated in RAL-ER dimers, but here, Path II′, suppressed in ER-E_2 dimers, was also detected.

The present study supports our previous proposal that NR-LBDs harbor multiple ligand escape pathways and is the first to examine effects of NR quaternary state on ligand escape paths; other studies employed monomeric LBD structures (18–22). Seminal LES studies of Karplus and co-workers (18) used monomeric models of RAR-LBD in vacuum and detected ligand escape through the mousetrap model. We used multiple crystallographic structures and larger number of simulations and observed an ensemble of escape paths in TR monomers (21, 22). An independent investigation of ligand escape from RAR using another simulation technique supported the notion that these receptors also harbor multiple ligand escape routes (20). RAR and TR systems were also investigated in steered MD simulations, pioneered by Schulten and collaborators (19), in which an external force is applied to the ligand in structural models to promote release along specific routes chosen by the researcher. Schulten and associates (19) tested three plausible directions of retinoid dissociation from RARs, including the mousetrap, based on analysis of RAR structure, and we examined the complete ensemble of TR ligand escape trajectories predicted by LES studies (21, 22). Both studies confirm that LES identifies plausible escape paths and further suggest that one pathway (Path III) is energetically favored in aqueous environments for retinoic acid and thyroid hormones. It will be

Fig. 5. Main Structural Rearrangements of ER-LBD/E_2 in Dimeric State that Accompany E_2 Escape through Path I

The dimer partner with ligand copies is shown in *cartoon* representation. The other partner, with a single ligand, is shown in *white bulky trace* representation. In *black* are the structural elements involved in the cavity formation. The picture on the *left* shows a view of the crystallographic structure with these elements in first plane. The picture on the *right* is a snapshot of the simulation showing the rearrangements of these structures responsible for escape cavity formation.

interesting to perform steered MD to explore molecular details, relative importance, and energetics of the ensemble of putative ER ligand pathways in the context of monomers and dimers.

Our results raise several questions. Why does dimer formation suppress E_2 escape? Why do escape pathways vary with ligand? Why is Path I′ unique to RAL and why can RAL, but not E_2, escape through Path II′ in the ER dimer? Consideration of our MD simulations with details of ER atomic structure suggests answers to these questions.

The reason that dimerization suppresses E_2 release seems simple: the dimer surface occludes important Path II and Path II′ escape routes, directly and indirectly. Path II requires displacements of key helices that are actively involved in the dimerization surface. Although H7, the unfolding of which leads to Path II′ escape cavity formation, does not actively participate in the dimer surface, this pathway may be suppressed because H7 is in close contact to H8 from the dimerization surface. Thus, dimerization probably stabilizes H7 and the interaction between the H7–H8 and H2–H3 loops that enclose the Path II′ escape cavity.

Why does RAL favor Paths I and I′? This seems to be related to H12 position. In the agonist conformation, with E_2, H12 docks over H3, H5, and H11, and the conformation is stabilized by hydrophobic interactions with residues of the ligand binding pocket and specific interactions with H3. This position stabilizes H11 and

Fig. 6. Main Structural Rearrangements of ER-LBD/RAL in Monomeric State that Accompany RAL Escape

Drawing style follows that of Fig. 3. A, Formation of path I escape cavity involving the H12 unfolding. B, Formation of escape cavity associated with path I′ due to ligand copies reorientation after H12 unfolding.

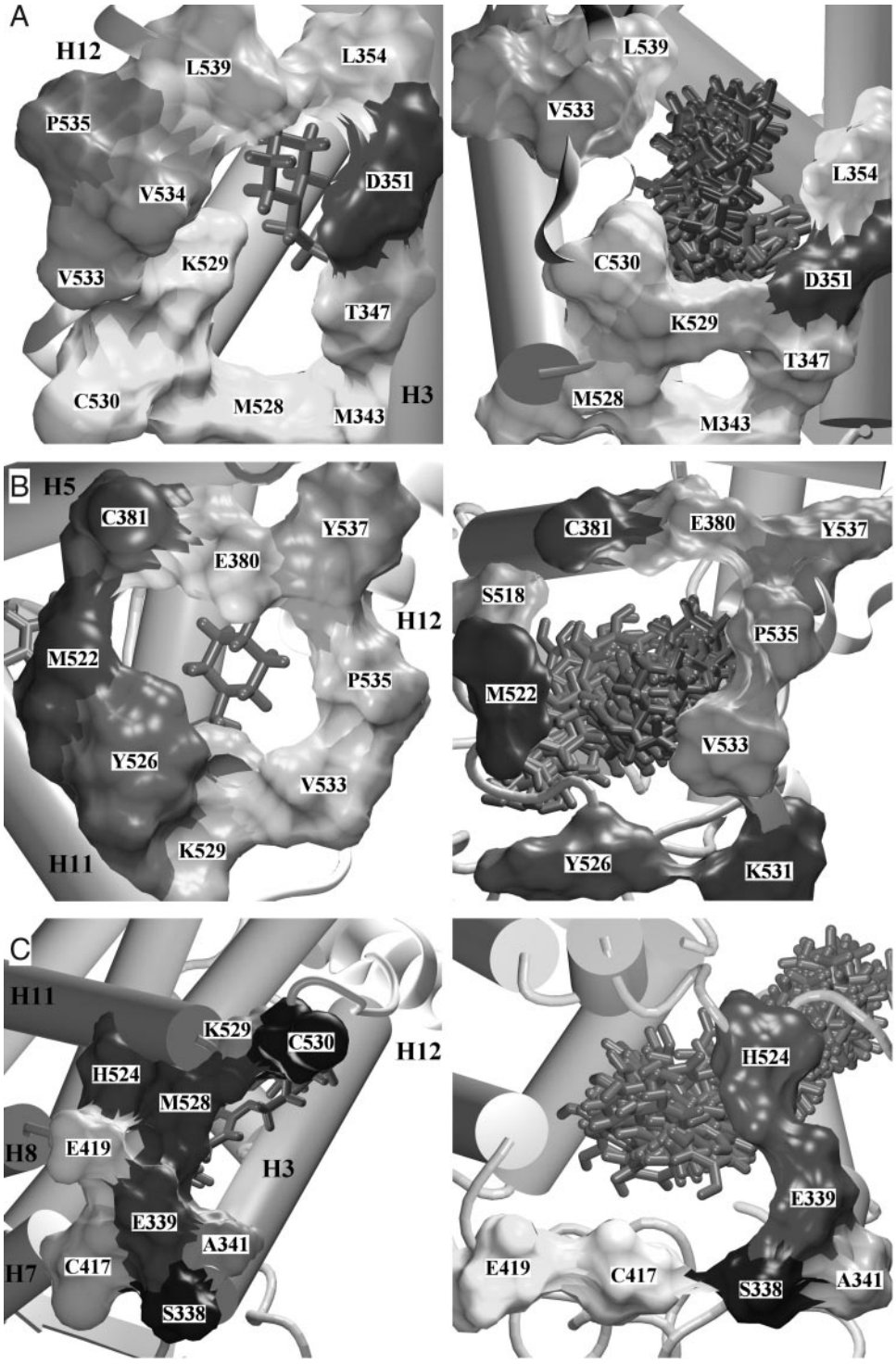

Fig. 7. Details of the RAL Escape Cavity Formation from ER-LBD

Drawing style follows that of Fig. 4. A, Cavity for escape through Path I. B, Cavity for escape through Path I′. C, Cavity for escape through Path II′. The last cavity was observed only in the dimeric system.

prevents melting and ligand escape through this region. In contrast, H12 is positioned over a coactivator-binding cleft in the antagonist conformation with RAL and is unable to contribute to H11 stabilization in the same fashion. Specific appearance of the variant Path I′ in MD simulations performed with RAL seems to be related to the fact that the RAL extension protrudes over H12, facilitating dissociation within H12 and H11.

Finally, why does dimer formation suppress E_2 dissociation through Paths II and II′ yet allow, or even

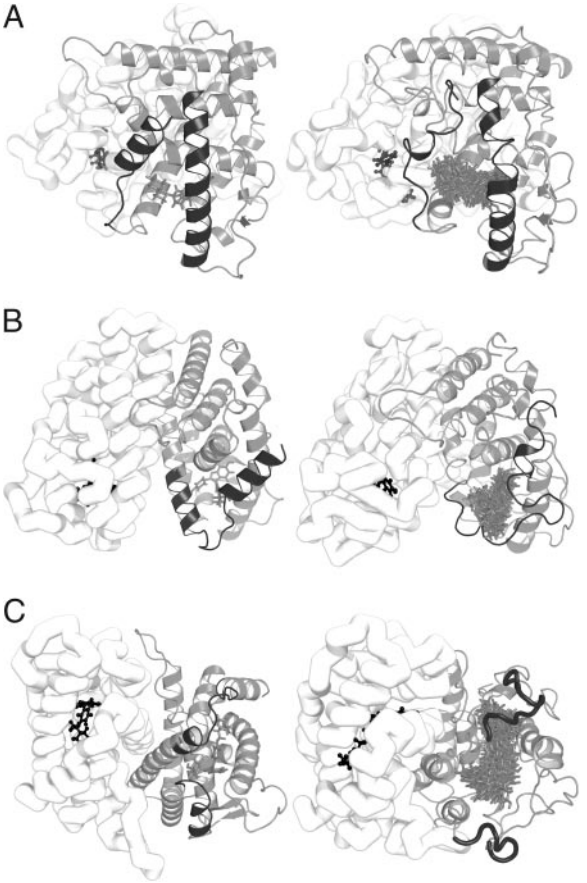

Fig. 8. Main Structural Rearrangements of ER-LBD/RAL in Dimeric State that Accompany RAL Escape

Drawing style follows that of Fig. 5. A, Escape cavity formation through Path I involving the H12 unfolding. B, Escape cavity formation through Path I′ due to ligand copies reorientation after partial H12 unfolding. C, Escape cavity formation through Path II′ at the *bottom* of the LBD structure, involving partial unfolding of the H7 and C terminus of H11.

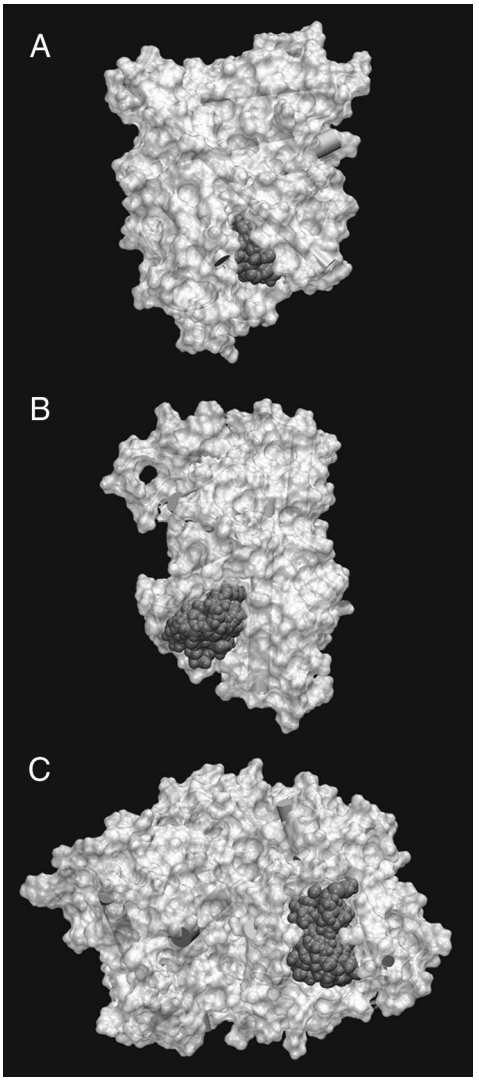

Fig. 9. Cavities on the Surface of the Protein Observed in Simulations Employing Full Explicit Solvation, Connecting the Ligand-Binding Pocket to the Surrounding Solvent Environment

Cavities are observed at the region of Path II and Path II′ in monomeric ERα-LBD/E_2 complex (panel A); at the region of Path I in monomeric ERα-LBD/RAL (panel B), and at the region of Path II′ in dimeric ERα-LBD/RAL (panel C).

promote, RAL dissociation through Path II"? A key event in Path II′ is detachment of the N terminus of H3 from H8 and H11. As described earlier, in *Results*, there are ligand-specific differences in secondary structural organization in this region. In the E_2 liganded ER structure the N terminus of H3 contacts the H11–H12 loop, whereas this contact is missing in the RAL-liganded structure. Two charged residues on H11 play important roles in the conformation of this region and choice of dissociation paths for dimers K520 and E523. In the dimer, glutamic acids of each LBD are near each other. In the E_2-liganded dimer, E523 oxygen atoms are 4.5 Å apart but turned toward the R548 in H12, attenuating their mutual electrostatic repulsion. In addition, carboxylate oxygens interact with solvent molecules permeating the dimerization interface. In the RAL-liganded dimer structure, however, the carboxylate groups cannot interact with R548 due to the H12 antagonist conformation, and glutamic acids face each other. Whereas part of the electrostatic repulsion is attenuated by a salt bridge with K520, Glu oxygen atoms are only 2.7 Å apart. Such proximity induces conformational changes of H11 in the RAL-ER dimer complex relative to the E_2-ER dimer that favor RAL release through this region.

The reasons that Path II′ was observed in RAL/ER-LBD dimers, but not monomers, are less clear. Perhaps competition between release paths impeded detection of Path II′ in monomer simulations. We note, however, that initial Path II′ ligand escape cavity involves partial unwinding of the C terminus of H11, increasing the length of the H11–H12 loop. Analysis of crystallographic structures of ER-SERM complexes reveals that this region adopts a loop-like conforma-

tion as opposed to well-defined helical structures observed with E_2 (10). Thus, SERM-dependent structural alteration could help ligand to escape through Path II′ (Figs. 7C and 8C). It will be interesting to determine whether this influence varies in monomers *vs.* dimers.

Current computing power limits the length of MD simulations, and manipulation of the system is needed to detect ligand escape in reasonable timescales. As mentioned earlier, LES involves simultaneous computation of multiple ligand interactions with the same protein and, in addition, we performed LES studies in vacuum, or with crystallographic waters only; addition of a solvation layer to simulate the cellular aqueous environment stabilizes receptor structure and eliminates ligand escape. Why do we think these adjustments allow for detection of plausible escape pathways? First, escape routes observed here exactly or closely resemble escape pathways previously detected for RARs and TRs in multiple types of MD simulations, including those with aqueous layers. Second, LES simulations of ER-LBDs in aqueous environments reveal transient formation of surface cavities that exactly correspond to the locations of escape routes detected *in vacuo*, implying that alterations in receptor structure in vacuum resemble those in simulated aqueous environments.

Previous experimental evidence corroborates our prediction of links between ER dimer formation to hormone dissociation. [^{3}H]E_2 dissociation from ER preparations that contain monomers and dimers are characterized by two half-lives; with fast (3.9–13.9 min) and slow (98–118 min) components (25). Dilution of ER preparations to obtain uniform monomers essentially eliminates the slower component whereas ER dimer preparations exhibit only the slow component (26). Moreover, equilibrium binding assays with ER preparations that contain dimers are characterized by high Hill coefficients (n_H 1.6–1.8), whereas ER monomers exhibit n_H values closer to 1.0. These findings provide compelling evidence that the fast component involves ER monomers and the slow component involves dimers. Because we detect three E_2 escape routes (Path I, II, and II′) and Paths II and II′ are suppressed in ER dimers, we propose that these routes could correspond to the rapid ligand release pathway and Path I, not suppressed by dimerization, corresponds to the slower release pathway. In this regard, our results are consistent with proposals of Zhong and Skafar (25), who argued that the ER-LBD monomer adopts a loose and mobile structure that allows ligand multiple escape pathways whereas the ER-LBD dimer is more stable and impedes formation of some escape cavities, resulting in slower ligand dissociation.

We recognize that there may be other explanations for biphasic ligand release kinetics. ER dimerization could exert indirect allosteric effects on H12, reducing hormone release through Path I. Alternatively, as Paths II and II′ depend strongly on dissociation of dimers into monomers, these paths could represent the major route of ligand release from both ER monomers and dimers with the slow component corresponding to dimers to monomer conversion. Indeed, studies using monomer exchange fluorescence resonant energy transfer revealed that the half-life of E_2/hER-LBD dimers is 150.8 $\pm$ 9.0 min at saturating E_2 concentrations (27), comparable to the slow component of E_2 dissociation from hER (up to 118 $\pm$ 4 min) (25).

Nevertheless, reexamination of other evidence supports the existence of multiple ligand release paths from ERs. For Path I, binding of coactivators and point mutations that stabilize H12 in the active conformation reduce ligand dissociation rates (28). One ER mutant, ERαY537S, however, slowed hormone association rate (k_{+1}) by a factor of approximately 6 times but only slowed the dissociation rate (k_{-1}) about 3-fold (29). Whereas reductions in association and dissociation rates are expected, *i.e*. the mutation stabilizes H12 in its active position, the fact that the ERY537S mutation selectively impairs ligand association could be consistent with the idea that there are competing dissociation paths not affected by H12, such as Path II or II′. Alanine scanning mutagenesis through H11, important in Path II, confirmed that the C-terminal region of H11 is important for E_2/ER affinity and that some residues, such as Y526 and M528, that are involved in Path II are required for optimal ligand binding (30). Perhaps observed changes are associated with changes in H11 conformation and dynamics that alter rates of ligand release through Path II.

Although our results corroborate the notion that NRs harbor multiple ligand release pathways, it was surprising that Path III, the likeliest pathway of ligand release for RARs and TRs in aqueous environments, failed to appear. This route involves H1–H3, and there is no obvious structural reason why this region is not available for ligand dissociation in ER monomer and dimer states. We propose instead that the absence of Path III is related to the nature of the ligand. RAR and TR ligands contain highly polar charged sites (carboxylate groups), which are oriented close to the Path III escape route in the pocket and interact with charged residues of the nearby β-sheet. Path III is preferred in TRs (21, 22); this is because ligand carboxylate-protein contacts are replaced by ligand interactions with external water molecules at little or no energetic cost, as opposed to Paths I and II for which breaking of ligand-protein hydrophilic contacts constitutes a barrier to ligand release (22). By contrast, E_2 exhibits a balanced charge distribution with hydroxyl groups at opposing extremities and a modest dipole moment of approximately 2.3 Debye, but no net charge or highly polar end (31) that could fulfill the role of the carboxylate groups.

Path II′, unique to ERs, was not detected for TRs and RARs. We propose that this is because this route involves melting of H7; TRs and RARs have large Ω-loops that connect H7 and 8 and make several contacts with H11 that would likely impair

ligand dissociation through the bottom of the LBD, whereas the ER N7–H8 loop is relatively short.

Of necessity, simulations were conducted in the absence of ER F-domain; this is absent in crystallographic models of ERs. The hERα F-domain is a 42-amino acid extension of H12 that is proposed to be flexible and possess an extended conformation approximately 100 Å long (32). X-ray structures of other steroid receptors (33–36) were resolved as monomers with the F-domain adopting a β-sheet structure that docks against the position of a key region of the ER dimer surface and, indeed, a number of investigations indicate that the human (h) ERα F-domain inhibits dimerization and interaction with coactivator proteins (32, 37–39). Whereas the F-domain could potentially protrude into solvent, it could also interact with different LBD surfaces, including the Path II′ region at the bottom of the LBD, the dimer interface, or even the dimer partner (32). Thus, F-domain position has the potential to influence monomer/dimer equilibrium, ligand dissociation kinetics, and escape routes from ER-LBD dimers in different ways. With antagonists, however, the F-domain would be positioned over H1, H2, H2–H3 loop, and H3 in the opposite direction of the dimer interface. This would not obviously clash with putative dissociation pathways, although it remains possible that it could confer greater stability to the LBD structure. In this regard, it may also be interesting to consider whether NR interdomain interactions could also alter ligand dissociation routes; however, lack of multidomain structures would make the present discussion about the effects of these interactions on ligand escape routes even more speculative.

In summary, our results suggest that there are multiple mechanisms for ligand association with, and dissociation from, ERs and other NRs and that the prevalence of particular pathways depends on receptor, ligand, quaternary state, and the presence or absence of associated cofactors. The fact that Paths II and II′ are sensitive to dimerization, and that Path II been observed in one other NR, the TR, raises the possibility that dimer formation could affect ligand dissociation for other receptors. We speculate that it may be possible to develop new pharmaceutically relevant ligands that could interact preferentially with specific NRs in specific oligomeric states and represent new types of selective modulators.

MATERIALS AND METHODS

LES Simulations

LES simulation techniques (40–43) are designed to sample molecular motions of a small subset (*e.g*. a ligand) of a given large molecular system (the ligand-protein complex) at reduced computational costs. To obtain a broader sampling of the structure and dynamics of the system, the subset of interest is replicated and the simulation is performed for the replicated set in the presence of a unique copy of the rest of the system. This method has been extensively used to study ligand diffusion through globins, and several results were confirmed experimentally (44–46). In a ligand-protein complex, for example, the ligand may be replicated several times. The ligand replicas do not interact with each other, and the interactions between individual ligand replicas and protein are scaled according to the number of replicas, such that the original (single) ligand-protein interaction is recovered on the average as long as the ligand replicas are nearly spatially overlapped. Because there are several copies of the ligand, the probability of observing a rare event (*e.g*. ligand dissociation) is increased. Furthermore, because the ligand-protein interactions are scaled by the number of copies, the energy barriers for dissociation of individual ligand replicas are also decreased, and therefore ligand dissociation rates are increased exponentially (41). This technique is particularly suitable to unravel likely dissociation pathways as opposed to attributing accurate likelihood to the individual paths. The biological relevance of the putative dissociation pathways obtained from LES simulations is inferred by correlating molecular aspects of the pathways with available experimental results from biophysical and functional assay studies.

There have been important theoretical developments to LES techniques (41–43) since the method was first proposed (40). Here, we have applied a fully Newtonian variation of the LES simulation method of Straub and Karplus (42) that we recently implemented and used for studying ligand dissociation from TRs (21). In our implementation, the masses of the ligand replicas are not scaled and the intramolecular potentials (bonded and nonbonded) for the ligands and for the protein amino acids are treated as full potentials. In this way, the dynamics of the system are fully Newtonian and the average kinetic energy per atom is $3k_BT/2$ independently of the number of copies used (energy equipartition is granted). Further details, drawbacks, and advantages of this implementation for simulating ligand-NR dissociation are presented elsewhere (21). It is important, however, to point out that unlike the approach of Ulitsky and Elber (43), the dynamics of our systems with multiple ligand copies do not fully map onto the dynamics of the original single-ligand problem and, therefore, the present approach does not yield reliable dissociation rates. Nevertheless, structural fluctuations and their features, which are the focus of the present work, are unaffected.

Parameterization of Ligands

Our simulations treat the ligands as fully flexible molecules. The van der Waals and torsional parameters for E_2 and RAL molecules were obtained by group analogy in the OPLS-AA set (47, 48). Partial atomic charges for these ligands were calculated from optimized structures at the Hartree-Fock 6–31G(d,p) level of theory with the Merz-Singh-Kollman electrostatic surface potential fitting protocol using Gaussian 98 (49). All the parameters for the ligands applied in the simulations of this work that are needed to re-run the calculations are provided as supplemental data published on The Endocrine Society's Journals Online web site at http://mend.endojournals.org.

MD Simulation Details

The vacuum simulations and in the presence of crystallographic waters were performed using TINKER (50), into which we have implemented our own subroutines for multiple ligand-copy LES Newtonian simulations. The initial configurations for E_2/ER-LBD and RAL/ER-LBD complexes in monomeric and dimeric states were obtained from Protein Data Bank (identifications, resolution and chains are as follows:

1ERE: 3.1 Å: chain A for E_2/ER monomer; 1QKU: 3.2 Å: chains B and C for E_2/ER dimer; 1ERR: 2.60 Å: chain A for RAL/ER monomer and chains A and B for RAL/ER dimer). Missing loops were modeled with MODELLER (51) (H2–H3 and H9–H10 in 1ERE, and H2–H3, H9–H10, and H11–H12 for 1ERR). When waters molecules were present, crystallographic waters within 5 Å to any protein or ligand atom were included. The TIP3P water model was employed. Individual hormone and protein atoms are explicitly treated, such that all atoms were included in the MD simulations. The potential energy parameters for the protein atoms were obtained from the OPLS-AA force field for protein simulation (47). Initial structures were minimized with the L-BFGS algorithm (52) to a final energy difference of 0.1 kcal/(mol.Å). These minimized structures were used as starting configurations for the MD simulations.

These systems comprised of one ligand per ER LBD unit in vacuum or with crystallographic waters; hence no periodic boundary conditions were applied. Initial random velocities from a Maxwell-Boltzmann distribution at temperature 25 C were assigned for each atom of the minimized structure, followed by *NVT* ensemble MD runs for structure relaxation lasting 100 psec using velocity Verlet algorithm with 1.0 fsec timestep and a Berendsen thermostat at 25 C with relaxation rate 1.0 $psec^{-1}$. Short-range van der Waals interactions were cut off at 10 Å. No cutoff was used for electrostatic interactions. Control simulations performed with these procedures on a similar ligand-NR system have shown the overall validity of our model (21). The LES simulations were then performed in the *NVE* ensemble starting from the thermalized structures in which the ligand is replaced by identical multiple copies with reassigned atomic random velocities corresponding to a temperature of 25 C. For the ER dimers, ligand replicas were placed only in one of the monomers of the dimer, keeping another LBD subunit with a single fully interacting ligand. The simulations were performed with different ligand copy numbers, varying from 20–50, to sample configurational space in searching for dissociation pathways in order that escape events could be observed within the duration of our simulations (~200 psec). Because dissociation rates are lower in the presence of crystallographic waters, we used 50 copies for the partially solvated systems.

For the fully solvated systems, a large number of TIP3P water molecules (~18,600 and 27,000 for monomers and dimers, respectively) was uniformly distributed around the protein-ligand complexes in addition to the crystallographic waters, forming a cubic box so that the boundaries are at least 15 Å away from any protein atom and the bulk solvent density far from the protein remained close to 1.0 g/cm^3. Chloride ions were added to achieve charge neutrality. Periodic boundary conditions were employed. van der Walls and electrostatic interactions were cut off at 12.0 Å, and a switching function starting at 10.0 Å was used. All systems were minimized by 5000 steps and subjected to 2.0 nsec of thermalization in the *NPT* ensemble with a time step of 2.0 fsec and Berendsen thermostat at 25 C with relaxation rate 1.0 $psec^{-1}$. A Berendsen barostat at 1 atm with water compressibility and relaxation rate of 0.01 $fsec^{-1}$ was also applied for thermalization. The end points of thermalization runs were used as starting configurations for the dissociation simulations using LES. All fully solvated systems were simulated using the NAMD molecular dynamics simulation package (53) with the maximum number of ligand copies, 15, allowed for in the NAMD code.

Although solvent effects are extremely important for proteins, the lack of solvent in most of our simulations is justified on the basis of two related aspects. First, the purpose of the present simulations is to investigate possible escape pathways of large ligand molecules (44 and 61 atoms for E_2 and RAL, respectively) from ER-LBDs and to identify early molecular events associated with the putative dissociation pathways. Second, the length of each LES simulation is less than 200 psec, and during this time interval the protein structure is largely preserved even in vacuum. Larger structural deformations are observed only in the later stages of the LES runs, when the ligand copies have essentially left the binding pocket. Indeed, the presence of solvent would decrease structural fluctuations of the protein and most likely prevent ligand escaping within this time scale. We have found that for retinoic acid dissociation from RAR, water molecules play an active role in stabilizing some interactions in the protein surface. However, we find that the same dissociation paths are encountered with and without structural water molecules, but the time scale of the dissociation is significantly increased in the presence of water (54). Moreover, recent results from random expulsion MD simulations have been reported for the dissociation of retinoic acid from RAR in the presence of a full hydration layer (20), which are consistent in many ways to the pioneering simulation studies of ligand dissociation from RAR (18, 19), one of which was performed in vacuum (18), and with our own LES study of dissociation from thyroid hormone receptors (21).

Acknowledgments

We thank the Laboratory of Advanced Scientific Computation of the University of São Paulo where most of the simulations were performed.

Received November 5, 2007. Accepted April 3, 2008.

Address all correspondence and requests for reprints to: Professor Igor Polikarpov, São Carlos Institute of Physics, University of São Paulo-USP, P.O. Box 369, São Carlos, SP 13560-970, Brazil. E-mail: ipolikarpov@ifsc.usp.br.

This work was supported by Fundação de Amparo à Pesquisa do Estado de São Paulo Grants 05/53931-5 (to M.T.S), 06/06831-8 (to L.M.), and 06/00182-8 (to M.S.S. and I.P.).

Disclosure Statement: The authors have nothing to disclose.

REFERENCES

1. Aranda A, Pascual A 2001 Nuclear hormone receptors and gene expression. Physiol Rev 81:1269–1304
2. Jordan VC 2003 Antiestrogens and selective estrogen receptor modulators as multifunctional medicines. 1. Receptor interactions. J Med Chem 46:883–908
3. Jordan VC 2003 Antiestrogens and selective estrogen receptor modulators as multifunctional medicines. 2. Clinical considerations and new agents. J Med Chem 46:1081–1111
4. Nilsson S, Gustafsson JA 2000 Estrogen receptor transcription and transactivation: basic aspects of estrogen action. Breast Cancer Res 2:360–366
5. Nilsson S, Koehler KF 2005 Oestrogen receptors and selective oestrogen receptor modulators: molecular and cellular pharmacology. Basic Clin Pharm Toxicol 96: 15–25
6. Muramatsu M, Inoue S 2000 Estrogen receptors: how do they control reproductive and nonreproductive functions? Biochem Biophys Res Commun 270:1–10
7. Gee AC, Katzenellenbogen JA 2001 Probing conformational changes in the estrogen receptor: evidence for a partially unfolded intermediate facilitating ligand binding and release. Mol Endocrinol 15:421–428
8. Tamrazi A, Carlson KE, Katzenellenbogen JA 2003 Molecular sensors of estrogen receptor conformations and dynamics. Mol Endocrinol 17:2593–2602
9. Gronemeyer H, Gustafsson JA, Laudet V 2004 Principles for modulation of the nuclear receptor superfamily. Nat Rev Drug Discovery 3:950–964

10. Nettles KW, Greene GL 2005 Ligand control of coregulator recruitment to nuclear receptors. Annu Rev Physiol 67:309–333
11. Moras D, Gronemeyer H 1998 The nuclear receptor ligand-binding domain: structure and function. Curr Opin Cell Biol 10:384–391
12. Nolte RT, Wisely GB, Westin S, Cobb JE, Lambert MH, Kurokawa R, Rosenfeld MG, Willson TM, Glass CK, Milburn MV 1998 Ligand binding and co-activator assembly of the peroxisome proliferator-activated receptor-γ. Nature 395:137–143
13. Wang L, Zuercher WJ, Consler TG, Lambert MH, Miller AB, Orband-Miller LA, McKee DD, Willson TM, Nolte RT 2006 X-ray crystal structures of the estrogen-related receptor-γ ligand binding domain in three functional states reveal the molecular basis of small molecule regulation. J Biol Chem 281:37773–37781
14. Kallen J, Schlaeppi JM, Bitsch F, Filipuzzi I, Schilb A, Riou V, Graham A, Strauss A, Geiser M, Fournier B 2004 Evidence for ligand-independent transcriptional activation of the human estrogen-related receptor α (ERR α)—Crystal structure of ERR α ligand binding domain in complex with peroxisome proliferator-activated receptor coactivator-1 α. J Biol Chem 279:49330–49337
15. Flaig R, Greschik H, Peluso-Iltis C, Moras D 2005 Structural basis for the cell-specific activities of the NGFI-B and the Nurr1 ligand-binding domain. J Biol Chem 280: 19250–19258
16. Baker KD, Shewchuk LM, Kozlova T, Makishima M, Hassell A, Wisely B, Caravella JA, Lambert MH, Reinking JL, Krause H, Thummel CS, Willson TM, Mangelsdorf DJ 2003 The *Drosophila* orphan nuclear receptor DHR38 mediates an atypical ecdysteroid signaling pathway. Cell 113:731–742
17. Wagner RL, Apriletti JW, Mcgrath ME, West BL, Baxter JD, Fletterick RJ 1995 A structural role for hormone in the thyroid-hormone receptor. Nature 378:690–697
18. Blondel A, Renaud JP, Fischer S, Moras D, Karplus M 1999 Retinoic acid receptor: a simulation analysis of retinoic acid binding and the resulting conformational changes. J Mol Biol 291:101–115
19. Kosztin D, Izrailev S, Schulten K 1999 Unbinding of retinoic acid from its receptor studied by steered molecular dynamics. Biophys J 76:188–197
20. Carlsson P, Burendahl S, Nilsson L 2006 Unbinding of retinoic acid from the retinoic acid receptor by random expulsion molecular dynamics. Biophys J 91:3151–3161
21. Martinez L, Sonoda MT, Webb P, Baxter JD, Skaf MS, Polikarpov I 2005 Molecular dynamics simulations reveal multiple pathways of ligand dissociation from thyroid hormone receptors. Biophys J 89:2011–2023
22. Martinez L, Webb P, Polikarpov I, Skaf MS 2006 Molecular dynamics simulations of ligand dissociation from thyroid hormone receptors: evidence of the likeliest escape pathway and its implications for the design of novel ligands. J Med Chem 49:23–26
23. Tamrazi A, Carlson KE, Rodriguez AL, Katzenellenbogen JA 2005 Coactivator proteins as determinants of estrogen receptor structure and function: spectroscopic evidence for a novel coactivator-stabilized receptor conformation. Mol Endocrinol 19:1516–1528
24. Ribeiro RCJ, Feng WJ, Wagner RL, Costa CHRM, Pereira AC, Apriletti JW, Fletterick RJ, Baxter JD 2001 Definition of the surface in the thyroid hormone receptor ligand binding domain for association as homodimers and heterodimers with retinoid X receptor. J Biol Chem 276: 14987–14995
25. Zhong L, Skafar DF 2002 Mutations of tyrosine 537 in the human estrogen receptor-α selectively alter the receptor's affinity for estradiol and the kinetics of the interaction. Biochemistry 41:4209–4217
26. Weichman BM, Notides AC 1977 Estradiol-binding kinetics of activated and non-activated estrogen-receptor. J Biol Chem 252:8856–8862
27. Tamrazi A, Carlson KE, Daniels JR, Hurth KM, Katzenellenbogen JA 2002 Estrogen receptor dimerization: ligand binding regulates dimer affinity and dimer dissociation rate. Mol Endocrinol 16:2706–2719
28. Gee AC, Carlson KE, Martini PGV, Katzenellenbogen BS, Katzenellenbogen JA 1999 Coactivator peptides have a differential stabilizing effect on the binding of estrogens and antiestrogens with the estrogen receptor. Mol Endocrinol 13:1912–1923
29. Carlson KE, Choi I, Gee A, Katzenellenbogen BS, Katzenellenbogen JA 1997 Altered ligand binding properties and enhanced stability of a constitutively active estrogen receptor: evidence that an open pocket conformation is required for ligand interaction. Biochemistry 36: 14897–14905
30. Ekena K, Weis KE, Katzenellenbogen JA, Katzenellenbogen BS 1996 Identification of amino acids in the hormone binding domain of the human estrogen receptor important in estrogen binding. J Biol Chem 271:20053–20059
31. Kubli-Garfias C 1998 Comparative study of the electronic structure of estradiol, epiestradiol and estrone by ab initio theory. Theochem J Mol Struct 452:175–183
32. Skafar DF, Koide S 2006 Understanding the human estrogen receptor-α using targeted mutagenesis. Mol Cell Endocrinol 246:83–90
33. Bledsoe RK, Madauss KP, Holt JA, Apolito CJ, Lambert MH, Pearce KH, Stanley TB, Stewart EL, Trump RP, Willson TM, Williams SP 2005 A ligand-mediated hydrogen bond network required for the activation of the mineralocorticoid receptor. J Biol Chem 280:31283–31293
34. Sack JS, Kish KF, Wang CH, Attar RM, Kiefer SE, An YM, Wu GY, Scheffler JE, Salvati ME, Krystek SR, Weinmann R, Einspahr HM 2001 Crystallographic structures of the ligand-binding domains of the androgen receptor and its T877A mutant complexed with the natural agonist dihydrotestosterone. Proc Natl Acad Sci USA 98:4904–4909
35. Kauppi B, Jakob C, Farnegardh M, Yang J, Ahola H, Alarcon M, Calles K, Engstrom O, Harlan J, Muchmore S, Ramqvist AK, Thorell S, Ohman L, Greer J, Gustafsson JA, Carlstedt-Duke J, Carlquist M 2003 The three-dimensional structures of antagonistic and agonistic forms of the glucocorticoid receptor ligand-binding domain: RU-486 induces a transconformation that leads to active antagonism. J Biol Chem 278:22748–22754
36. Williams SP, Sigler PB 1998 Atomic structure of progesterone complexed with its receptor. Nature 393:392–396
37. Koide A, Zhao CQ, Naganuma M, Abrams J, Deighton-Collins S, Skafar DF, Koide S 2007 Identification of regions within the F domain of the human estrogen receptor α that are important for modulating transactivation and protein-protein interactions. Mol Endocrinol 21: 829–842
38. Montano MM, Muller V, Trobaugh A, Katzenellenbogen BS 1995 The carboxy-terminal F-domain of the human estrogen-receptor: role in the transcriptional activity of the receptor and the effectiveness of antiestrogens as estrogen antagonists. Mol Endocrinol 9:814–825
39. Peters GA, Khan SA 1999 Estrogen receptor domains E and F: role in dimerization and interaction with coactivator RIP-140. Mol Endocrinol 13:286–296
40. Elber R, Karplus M 1990 Enhanced sampling in molecular-dynamics—use of the time-dependent Hartree approximation for a simulation of carbon-monoxide diffusion through myoglobin. J Am Chem Soc 112:9161–9175
41. Ulitsky A, Elber R 1993 The thermal-equilibrium aspects of the time-dependent Hartree and the locally enhanced sampling approximations—formal properties, a correc-

tion, and computational examples for rare-gas clusters. J Chem Phys 98:3380–3388
42. Straub JE, Karplus M 1991 Energy equipartitioning in the classical time-dependent Hartree approximation. J Chem Phys 94:6737–6739
43. Ulitsky A, Elber R 1994 Application of the locally enhanced sampling (LES) and a mean-field with a binary collision correction (Cles) to the simulation of Ar diffusion and no recombination in myoglobin. J Phys Chem 98: 1034–1043
44. Gibson QH, Regan R, Elber R, Olson JS, Carver TE 1992 Distal pocket residues affect picosecond ligand recombination in myoglobin—an experimental and molecular-dynamics study of position 29 mutants. J Biol Chem 267:22022–22034
45. Scott EE, Gibson QH, Olson JS 2001 Mapping the pathways for O-2 entry into and exit from myoglobin. J Biol Chem 276:5177–5188
46. Brunori M, Gibson QH 2001 Cavities and packing defects in the structural dynamics of myoglobin. EMBO Rep 2:674–679
47. Kaminski GA, Friesner RA, Tirado-Rives J, Jorgensen WL 2001 Evaluation and reparametrization of the OPLS-AA force field for proteins via comparison with accurate quantum chemical calculations on peptides. J Phys Chem B 105:6474–6487
48. Jorgensen WL, Maxwell DS, TiradoRives J 1996 Development and testing of the OPLS all-atom force field on conformational energetics and properties of organic liquids. J Am Chem Soc 118:11225–11236
49. Frisch MJ, Trucks GW, Schlegel HB, Scuseria GE, Robb MA, Cheeseman JR, Montgomery Jr JA, Vreven T, Kudin KN, Burant JC, Millam JM, Iyengar SS, Tomasi J, Barone V, Mennucci B, Cossi M, Scalmani G, Rega N, Petersson GA, Nakatsuji H, Hada M, Ehara M, Toyota K, Fukuda R, Hasegawa J, *et al*. 2004 Gaussian 03, revision C.02, Gaussian, Inc., Wallingford CT
50. Ponder JW 2004 TINKER Software Tools for Molecular Design, version 4.2
51. Sali A, Blundell TL 1993 Comparative protein modeling by satisfaction of spatial restraints. J Mol Biol 234: 779–815
52. Liu DC, Nocedal J 1989 On the limited memory Bfgs method for large-scale optimization. Math Program 45: 503–528
53. Phillips JC, Braun R, Wang W, Gumbart J, Tajkhorshid E, Villa E, Chipot C, Skeel RD, Kale L, Schulten K 2005 Scalable molecular dynamics with NAMD. J Comput Chem 26:1781–1802
54. Sonoda MT, Moreira NH, Martinez L, Favero FW, Vechi SM, Martins LR, Skaf MS 2004 A review on the dynamics of water. Braz J Physics 34:3–16

Molecular Endocrinology **is published monthly by The Endocrine Society (http://www.endo-society.org), the foremost professional society serving the endocrine community.**